

# Journal of Materials Chemistry C

Accepted Manuscript



This is an *Accepted Manuscript*, which has been through the Royal Society of Chemistry peer review process and has been accepted for publication.

*Accepted Manuscripts* are published online shortly after acceptance, before technical editing, formatting and proof reading. Using this free service, authors can make their results available to the community, in citable form, before we publish the edited article. We will replace this *Accepted Manuscript* with the edited and formatted *Advance Article* as soon as it is available.

You can find more information about *Accepted Manuscripts* in the [Information for Authors](#).

Please note that technical editing may introduce minor changes to the text and/or graphics, which may alter content. The journal's standard [Terms & Conditions](#) and the [Ethical guidelines](#) still apply. In no event shall the Royal Society of Chemistry be held responsible for any errors or omissions in this *Accepted Manuscript* or any consequences arising from the use of any information it contains.

Cite this: DOI: 10.1039/c0xx00000x

www.rsc.org/xxxxxx

Paper

# Improved electrochromic performance and lithium diffusion coefficient in three-dimensionally ordered macroporous V<sub>2</sub>O<sub>5</sub> films

Zhongqiu Tong<sup>a</sup>, Jian Hao<sup>b</sup>, Kun Zhang<sup>b</sup>, Jiupeng Zhao<sup>b,\*</sup>, Bao-Lian Su<sup>c</sup>, Yao Li<sup>a,\*</sup>

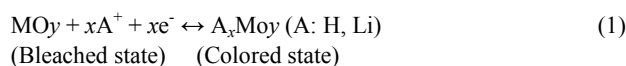
Received (in XXX, XXX) Xth XXXXXXXXX 20XX, Accepted Xth XXXXXXXXX 20XX

DOI: 10.1039/b000000x

Three-dimensionally ordered macroporous (3DOM) vanadium pentoxide (V<sub>2</sub>O<sub>5</sub>) films with various pore diameters were prepared by anodic deposition into colloidal crystal templates. The influence of the 3DOM structure on lithium ion (Li<sup>+</sup>) diffusion coefficient was investigated for the first time. X-ray diffraction analysis and HRTEM measurements show the skeleton walls are composed of crystallites and amorphous V<sub>2</sub>O<sub>5</sub>. The study of electrochromic properties indicates that pore size has significant impact on the electrochromic performance. Small pores in the film lead to higher optical contrast and faster switching response. A high transmittance modulation in the visible and near-infrared spectral regions (50 % at λ = 650 nm and 47 % at λ = 900 nm) with fast response time (1.7 s for coloration and 3.2 s for bleaching) is observed in the 3DOM V<sub>2</sub>O<sub>5</sub> film with a pore size of 210 nm. Because of the fully interconnected macroporous network in 3DOM structure, the transport and reaction of lithium ions and electrons both behave in an effective 3D model throughout the whole nanostructure. Additionally, due to their influences on the polarization of the electrode and surface defects, sharp nanoscale edges around pores and rough surfaces can further promote Li<sup>+</sup> diffusion and intercalation/de-intercalation. The 3DOM V<sub>2</sub>O<sub>5</sub> film with a pore size of 210 nm exhibits a very high Li<sup>+</sup> diffusion coefficient of 3.78 × 10<sup>-9</sup> cm<sup>2</sup>/s, which is higher than any coefficient ever reported for a V<sub>2</sub>O<sub>5</sub> film.

## Introduction

Electrochromic materials have been attracting enormous attention because of their commercial applications in smart windows, display devices, controlled reflectance mirrors and spacecraft thermal control<sup>1-4</sup>. Because of their low operating potential, ~1 V, they require very small amounts of energy to change their coloration states. Furthermore, memory effect is another merit of these materials, which leads them to require little power to maintain their coloration states<sup>1</sup>. Typically, a conducting metal oxide film acts as the chromogenic electrode. Upon applying external potential changes, reversible electric-field-induced intercalation/de-intercalation of small ions (such as H<sup>+</sup> and Li<sup>+</sup>) into/from an chromogenic oxide lattice (e.g. WO<sub>3</sub>, TiO<sub>2</sub>, NiO and V<sub>2</sub>O<sub>5</sub>)<sup>5-8</sup>, leading to reversible changes in optical parameters.



This double injection of ions and electrons maintains the electroneutrality of the chromogenic electrode. Optical contrast, ΔT(λ), between bleached state and colored state is limited by the amount of accessible intercalation sites. Switching time, τ, between bleached state and colored state is restricted by the diffusion distance required to achieve satisfactory color saturation<sup>9-12</sup>. Conventional flat electrochromic films exhibit a solid surface with relatively long diffusion distances, leading to small number of active intercalation sites and long switching time<sup>13</sup>. Electrochromic materials in form of nanoparticles<sup>14, 15</sup>, nanorods<sup>16, 17</sup>, nanofibers<sup>18-20</sup> or nanoscale clusters<sup>8, 21</sup> exhibited

significantly improved performance. However, because these kinds of electrochromic materials are always in powder form, additional processing is needed to attach them to a transparent current collector (e.g., ITO, FTO). Additionally, weak physical adhesion strength among individual electrochromic nanomaterials may cause the release of active materials, resulting in optical contrast loss in long-term testing<sup>22</sup>. A simple and effective way to solve this problem is the formation of a nanoscale network structure directly on transparent current collector<sup>23-25</sup>.

Three-dimensionally ordered macroporous (3DOM) structure, with an interconnected network of nanometer thick walls, is an attractive architecture for electrochromic materials<sup>26-28</sup>. In a 3DOM material, the bicontinuous structure provides intercontinuous pore spaces for good electrolyte penetration, while the continuous walls give effective transports pathway for electron and ion conduction<sup>22, 27, 28</sup>. Typically, a 3DOM structure is obtained by replicating the structure of a colloidal crystal template stacked by microspheres<sup>29-33</sup>. Thus, a 3DOM structure presents a high surface-area-to-volume ratio with nanometer-sized walls for short diffusion lengths and high active surface area for large number of intercalation sites. In addition, when a colloidal crystal template is assembled on a current collector, the prepared 3DOM electrochromic material exhibits strong adhesion to the current collector. Because of these advantages, colloidal-crystal-template materials of various oxides with 3DOM structure have been prepared for high-performance electrochromic devices<sup>31-34</sup>, supercapacitors<sup>35, 36</sup>, lithium ion batteries<sup>22, 37</sup>, solar cells<sup>38</sup>, and fuel cells<sup>39</sup>. However, to our best knowledge, reports of ion diffusion behaviors, especially regarding Li<sup>+</sup> diffusion coefficients, in 3DOM structures have rarely been published.

Because 3DOM structures are widely used in energy storage and conversion applications (e.g. electrochromism, lithium ion batteries, supercapacitors), the study of  $\text{Li}^+$  ion diffusion coefficients in 3DOM structures is necessary to better understand how this kind of morphology improves performance.

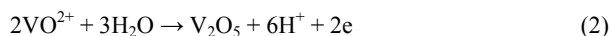
Vanadium pentoxide ( $\text{V}_2\text{O}_5$ ), with a layered structure, is a promising material for electrochromic applications<sup>7, 18, 23, 24</sup> because of the observed reversible  $\text{Li}^+$  ion intercalation/de-intercalation between its layers<sup>40-42</sup>. However, the inherently low  $\text{Li}^+$  diffusion coefficients ( $10^{-13} - 10^{-12} \text{ cm}^2/\text{s}$ ) and moderate electrical conductivity ( $10^{-3} - 10^{-2} \text{ S/cm}$ ) of  $\text{V}_2\text{O}_5$  materials<sup>43, 44</sup> have limited their lithium ion intercalation properties.

Here, anodic deposition of  $\text{V}_2\text{O}_5$  into colloidal crystal templates was used to prepare 3DOM  $\text{V}_2\text{O}_5$  films with pores of various sizes. The effects of the resulting structural differences on  $\text{Li}^+$  diffusion coefficients were studied. Optical contrast in the visible and NIR spectral ranges is greatly enhanced, reaching 50 % transmission contrast at  $\lambda = 650 \text{ nm}$  and 47 % at  $\lambda = 900 \text{ nm}$  in the 3DOM  $\text{V}_2\text{O}_5$  film with pore size of 210 nm. In 3DOM structure, both lithium ions and electrons are transported in a 3-dimensionally bicontinuous model. The 3DOM  $\text{V}_2\text{O}_5$  film with 210 nm pores exhibited a high  $\text{Li}^+$  diffusion coefficient of  $3.78 \times 10^{-9} \text{ cm}^2/\text{s}$ , similar to that observed in a carbon nanotube/ $\text{V}_2\text{O}_5$  composite ( $3 \times 10^{-9} \text{ cm}^2/\text{s}$ )<sup>45</sup>. The results presented here provide an opportunity to address the fundamental studies of 3DOM structure for advanced electrochromics and energy storage/conversion applications.

## Experimental section

Monodispersed polystyrene (PS) latex spheres (diameters of 210, 340, and 840 nm) were obtained using emulsifier-free emulsion polymerization technology<sup>46</sup>. PS colloidal crystal templates were grown using a controlled vertical drying method<sup>46</sup>. Indium-doped tin oxide substrates (ITO,  $\sim 9 \Omega/\text{cm}^2$ ,  $1 \text{ cm} \times 3 \text{ cm}$ ) were cleaned ultrasonically in acetone, then methanol, and then distilled water, for 20 min each. The cleaned ITO glass substrates were placed into cylindrical vessels. PS sphere suspension diluted to 0.5 wt% was added into glass vessels and then evaporated in an incubator at a stable temperature of 60 °C.

Anodic deposition of  $\text{V}_2\text{O}_5$  into polystyrene colloidal crystal templates was performed at a constant voltage of 2 V versus Ag/AgCl from a 1:1 mixture (volume ratio) of distilled water and ethanol containing 0.25 M  $\text{VOSO}_4 \cdot 5\text{H}_2\text{O}$  and a Pt foil as counter electrode. Ethanol was used to reduce the surface tension between the electrolyte and the polystyrene surface. The pH of the electrolyte was adjusted to 2.7 using NaOH. Oxidation of  $\text{VO}^{2+}$  and deposition of  $\text{V}_2\text{O}_5$  proceeded through the following reaction at a pH between 2.4 and 2.7<sup>43</sup>:



After deposition, samples were immersed in a 1:1 mixture (volume ratio) of DMF and toluene for 24 h to remove the polystyrene templates. Finally, the as-prepared samples were dried at 110 °C for 3 h and then annealed in air at 275 °C for 4 h. For the sake of comparison, a dense  $\text{V}_2\text{O}_5$  film was also prepared without template.

The morphologies of the 3DOM  $\text{V}_2\text{O}_5$  films were characterized

by scanning electron microscopy (SEM, FEI Helios Nanolab 600i). Crystalline structures of the  $\text{V}_2\text{O}_5$  films was investigated by a rotation anode X-ray diffractometer (Japan Rigaku DMax-rb) with a graphite monochromatized Cu K $\alpha$  radiation (0.15418 nm) and High Resolution Transmission Electron Microscopy (HRTEM, FEI Tecnai G2F30, 300 kV). *In situ* visible and near-IR (NIR) electrochromic measurements were performed using an experimental setup produced in-house (same setup used in Ref. 47) in combination with a CHI 660C electrochemical workstation (Shanghai Chenhua Instrument Co. Ltd.). The experimental setup was sealed in an Argon-filled glove box (Vigor Glove Box from Suzhou, China) before testing. One side of the setup was connected to a white lamp (DT-mini-2-GS, Ocean Optics) by an optical fiber; the other side was connected to an optic spectrometer (MAYA 2000-Pro, Ocean Optics). The  $\text{V}_2\text{O}_5$  film, Pt wire, and Ag/AgCl were used as working electrode, counter electrode, and reference electrode, respectively. A 1 M solution of  $\text{LiClO}_4$  in propylene carbonate was used as the electrolyte. The transmittance of the ITO glass in the electrolyte was used as a reference for 100 % transmittance. Before measuring the electrochromic performance of the  $\text{V}_2\text{O}_5$  films, the film electrodes were subjected to three cyclic voltammetry (CV) cycles to ensure stability. CV measurements were performed at room temperature between +1 and -1 V at a scan rate of 5 mV s<sup>-1</sup>. Chronoamperometric measurements were done by applying +1 V for 1000s to de-intercalate all lithium ions present, then setting the potential back to -0.5 V for 500s followed +0.5 V for 500s, and monitoring the current as a function of time during testing.

## Results and discussion

Fig. 1 shows top-view and cross-section SEM images of 3DOM  $\text{V}_2\text{O}_5$  films with different pore sizes. Due to replication of the 3D ordered structures of the colloidal crystal templates, all  $\text{V}_2\text{O}_5$  films grown directly on the conducting ITO layers displays highly periodic honeycomb structures with nanoscale walls throughout their entire volumes. The nanoscale walls can significantly decrease diffusion length of Li ions during electrochromic processes. Because of shrinkage during annealing, the macroporous structures become slightly deformed. Interestingly, cross-section SEM images of the 3DOM  $\text{V}_2\text{O}_5$  films indicate that two types of pores were present: large macropores with sizes similar to those of the PS spheres and smaller mesopores on the order of tens of nanometers, which formed at the contact points between spheres. Such a hierarchical porous structure is expected to not only provide continuous pathways for electron transport, but also to increase the number of possible intercalation sites. The thicknesses of all 3DOM films obtained were  $1.1 \pm 0.1 \mu\text{m}$ , indicating the almost same solid volume in the 3DOM  $\text{V}_2\text{O}_5$  films but different surface area. In contrast, the  $\text{V}_2\text{O}_5$  film prepared without a template showed a homogeneously dense structure. For the comparison, similar thickness of dense  $\text{V}_2\text{O}_5$  film was prepared.

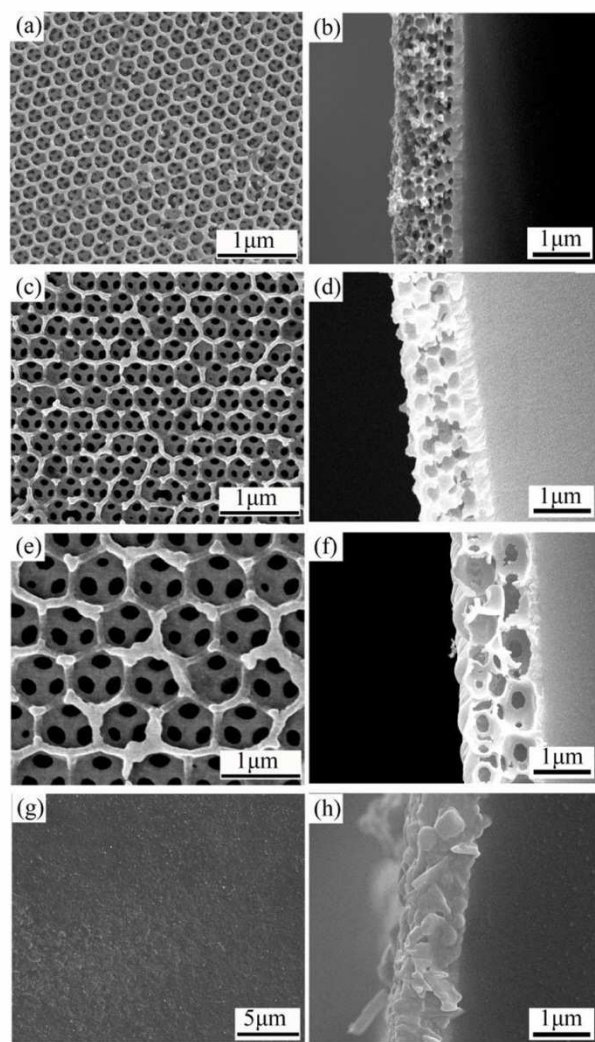


**Fig. 1** Typical top-view and cross-section SEM images of 3DOM  $V_2O_5$  films with various pore sizes: (a) and (b) 210 nm, (c) and (d) 340 nm, and (e) and (f) 840 nm. SEM images of the dense  $V_2O_5$  film are shown in (g) and (h).

X-ray diffraction patterns of the 3DOM and the dense  $V_2O_5$  films are shown in Fig. 2a. In addition to the diffraction peaks of the ITO glass, the 3DOM  $V_2O_5$  films shows both broad diffraction peaks and distinct sharp peaks, indicating that the 3DOM network is a mixture of crystalline and amorphous  $V_2O_5$ . The two X-ray diffraction peaks at  $2\theta = 20.1^\circ$  and  $41.2^\circ$  are assigned to the (001) and (002) planes of orthorhombic phase  $V_2O_5$  (JCPDS 41-1426). The crystallite sizes calculated from the Scherrer Equation are 17 nm, 15 nm, and 21 nm for the 3DOM  $V_2O_5$  films with pore size of 210 nm, 340 nm, and 840 nm, respectively. In contrast, no crystalline  $V_2O_5$  diffraction peaks are found in the dense film. To further analyze the crystalline structure in the nanostructured walls, the bright-field HRTEM image and selected-area electron diffraction (SAED) pattern for 3DOM  $V_2O_5$  film with pore size of 210 nm are obtained in Fig. 2b. The HRTEM image clearly shows that the walls are composed of nanocrystals and amorphous parts. The observed lattice spacing is about 0.217 nm, which corresponds to the distance between the (002) crystal planes of the orthorhombic  $V_2O_5$  phase. The SAED pattern

(inserted in Fig. 2b) reveals a set of diffraction rings typical for nanocrystalline orthorhombic  $V_2O_5$ , in agreement with the XRD results. It can be concluded that the confined deposition of  $V_2O_5$  into the voids of PS colloidal crystal templates improves the crystallinity of the deposited film. Our following publication will show majority of the crystalline particles are near the surface of 3DOM skeleton wall surface. Typically, the increasing crystallinity can significantly improve electrical conductivity<sup>22, 48</sup>, which is important for effective electrochromic reactions<sup>22, 23</sup>. Thus, 3DOM structures can enhance electrochromic performance by improving film crystallinity.

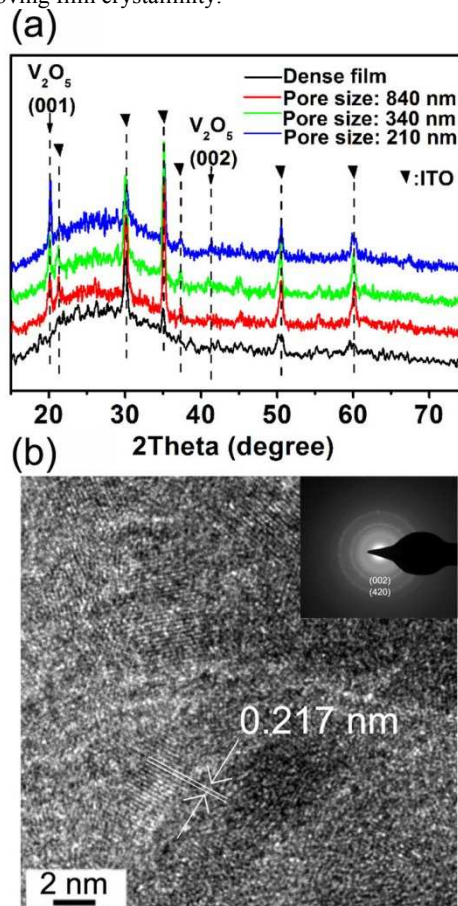


**Fig. 2** (a) XRD patterns of the 3DOM  $V_2O_5$  films of various pore sizes as well as a dense  $V_2O_5$  film; (b) HRTEM image and SAED pattern of 3DOM  $V_2O_5$  films of pore size of 210 nm

Fig. 3 presents the CV curves of three 3DOM films and the dense  $V_2O_5$  film obtained at a scan rate of  $5 \text{ mV s}^{-1}$  using 1 M  $\text{LiClO}_4$  propylene carbonate electrolyte and a potential window of  $\pm 1 \text{ V}$ . Over this potential range, the 3DOM  $V_2O_5$  films exhibits four couples of redox peaks, which are assigned to phase transitions between the  $\alpha$ ,  $\epsilon$ ,  $\delta$ ,  $\gamma$ , and  $\omega$  phases, according to the literature<sup>24, 49, 50</sup>. The above lithium ion intercalation processes are accompanied by color changes. For the 3DOM  $V_2O_5$  films, films with smaller pore sizes exhibit larger current densities, indicating larger active surface areas and shorter ion diffusion distances, making the electrochromic reaction more effective. The effect of pore size on the electrochromic properties can also be shown by analysis of the CV redox peaks. The current intensities of the  $\delta/\gamma$  and  $\gamma/\omega$  phase-transition peaks decreased with increasing pore

size, implying ineffective  $\text{Li}^+$  intercalation reactions in 3DOM  $\text{V}_2\text{O}_5$  films with larger pores. Only two broad featureless peaks are associated with the dense film, compared to the four of the 3DOM films, indicating poor  $\text{Li}^+$  intercalation/de-intercalation in the dense film. It is noteworthy that the 3DOM  $\text{V}_2\text{O}_5$  films exhibits four apparent couples of redox peaks, indicating their lithium ion intercalation/de-intercalation processes to be much more reversible than those of the dense film<sup>24, 49</sup>. In the case of that the colloidal crystal templates are face-centered cubic (fcc) arrays, the duplicated 3DOM films show almost same solid volume but different active surface areas and  $\text{Li}^+$  diffusion distances. The surface area of a 3DOM  $\text{V}_2\text{O}_5$  film depends on the number of stacked sphere layers. Thus, the surface-area ratio was about 6: 3: 2 in the 3DOM films with pore size of 210 nm, 340 nm, and 840 nm. Taking the dense film into account, the surface-area ratio of 3DOM films with different pores to dense film was 6: 3: 2: 1. The influence of pore size on the thickness of nanostructured walls can be deduced from the polyhedral position in 3DOM structure. In 3DOM structure, the maximum wall size situates at the octahedral position, derived from octahedral voids of colloidal crystals. The maximum size of octahedral voids is  $0.414R/2$ , where  $R$  equals the diameter of microspheres. Because of the difference in the diameters of stacked microspheres, the duplicated 3DOM structure  $\text{V}_2\text{O}_5$  films present different wall sizes. In the case of dense  $\text{V}_2\text{O}_5$  film, the  $\text{Li}^+$  diffusion distance is the thickness of the prepared film. Because of multiple and reversible electrochemical reactions, these 3DOM films have significant potential in electrochromism and other ion intercalation applications, such as supercapacitors and lithium ion batteries.

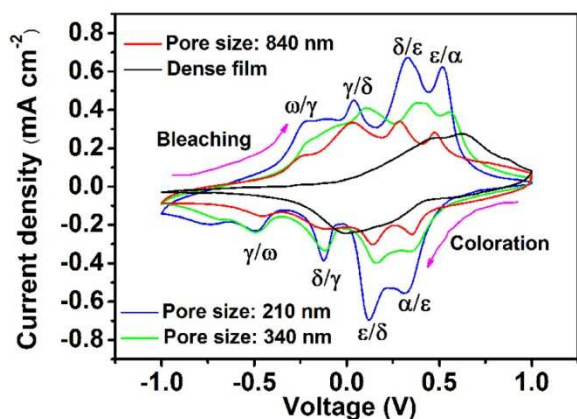


**Fig. 3** CV curves of the 3DOM  $\text{V}_2\text{O}_5$  films as well as the dense  $\text{V}_2\text{O}_5$  film, obtained at a rate of  $5 \text{ mV s}^{-1}$ , in  $1 \text{ M LiClO}_4$  propylene carbonate electrolyte.

*In situ* visible and NIR transmittance measurements were used to investigate the effects of the 3DOM structure on electrochromic performance. Both the 3DOM films and the dense film were colored by applying a constant voltage of  $-1 \text{ V}$  (vs.  $\text{Ag}/\text{AgCl}$ ) for 40 s and bleached at  $1 \text{ V}$  (vs.  $\text{Ag}/\text{AgCl}$ ) for 40 s. Fig. 4a and 4b show the transmittance modulation ( $\Delta T$ ) of the 3DOM films and the dense film, respectively. All of the 3DOM films show larger  $\Delta T$  values than dose the dense film over the entire spectral region and the  $\Delta T$  values of the 3DOM films decrease with increasing pore size. By combining larger active surface areas and shorter

$\text{Li}^+$  diffusion distances for more effective  $\text{Li}^+$  intercalation, with smaller crystalline grains for electron transport, 3DOM  $\text{V}_2\text{O}_5$  films with smaller pores exhibits better transmittance modulations. The  $\Delta T$  values obtained at wavelengths of 450, 650, and 900 nm are listed in Table 1. For the 3DOM  $\text{V}_2\text{O}_5$  film with a pore size of 210 nm, a 50 % transmission contrast is reached when  $\lambda = 650 \text{ nm}$ , which is comparable to the 3D interconnected porous  $\text{V}_2\text{O}_5$  film prepared from a voided double-gyroid copolymer template (approximately 50 %) and much higher than a  $\text{V}_2\text{O}_5$  film randomly stacked with  $\text{V}_2\text{O}_5$  nanowires (approximately 20 %) <sup>18</sup>. In the 3DOM structured films, lithium intercalation into  $\text{V}_2\text{O}_5$  under a cathodic potential of  $-1 \text{ V}$  causes a fairly homogeneous transmission of *ca.* 40 % across the entire visible range, resulting in a dark grey coloration (Fig. 4d). Charge extraction under an anodic potential of  $+1 \text{ V}$  causes a strong absorption in the 400-500 nm spectral range, leading to a yellow color (Fig. 4d). Optical density ( $\Delta OD$ ) is an important parameter for the evaluation of an electrochromic material's optical modulation ability [32]. Optical density can be defined as

$$\Delta OD_\lambda = \log(T_{bl}/T_{cl}) \quad (7)$$

where  $T_{bl}$  and  $T_{cl}$  represent the transmittance of the bleached and colored sample, respectively. As show in Fig. 4c, the 3DOM films exhibit higher optical modulation ability than the dense film over the entire spectral region, and the  $\Delta OD$  of the 3DOM films increases with decreasing pore size.

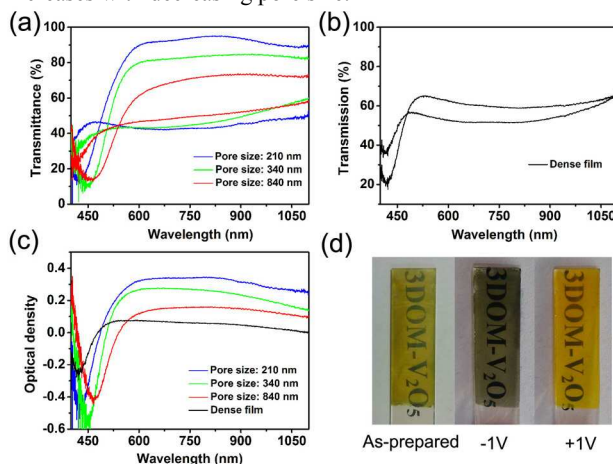


**Fig. 4** Transmittance contrast of (a) the 3DOM  $\text{V}_2\text{O}_5$  films and (b) the dense  $\text{V}_2\text{O}_5$  film; (c) optical density of both the 3DOM and the dense films, and (d) electrochromic digital photographs of a 3DOM  $\text{V}_2\text{O}_5$  film with pore size of 210 nm, under different potentials.

**Table 1.** Optical characteristics of 3DOM  $\text{V}_2\text{O}_5$  films and dense  $\text{V}_2\text{O}_5$  film

Sample	$\Delta T$ at different wavelength (%)		
	at 450 nm	at 650 nm	at 900 nm
Pore diameter: 210 nm	24	50	47
Pore diameter: 340 nm	26	38	30
Pore diameter: 840 nm	19	19	18
Dense film	16	10	4

A second important aspect of electrochromism is the temporal spectral response under alternating potentials. Alternating potentials lead to alternating intercalation/de-intercalation of  $\text{Li}^+$  ions, resulting in coloration/bleaching switching<sup>1-3</sup>. Switching

behavior was analyzed by monitoring the transmittance at a wavelength of 800 nm under the application of a square wave voltage between +1 V and -1 V. Switching time is defined as the time required reaching 90 % of a material's full transmittance change. Fig. 5 shows the transmittance-time response of the  $V_2O_5$  films. The 3DOM films exhibits sharp changes during potential transitions, while the dense film shows gradual changes. This phenomenon clearly indicates that 3DOM films have much faster response times than the dense film. Characteristic switching times are listed in Table 2. From Table 2, it can be seen that the coloration and bleaching switching responses of all of the 3DOM films are enhanced with respect to the dense film. By combining these values with transmittance change values, response times of coloration and bleaching are found to be only 1.7 s and 3.2 s, respectively, for the 3DOM film with a pore size of 210 nm. Contrarily, the coloration and bleaching times of the dense film are 13.1 s and 13.5 s, respectively. In addition, the response time of the 3DOM  $V_2O_5$  film with a pore size of 210 nm is much shorter than that of  $V_2O_5$  nanowire stacked film<sup>51</sup>, which required 6 s for coloration and 5 s for bleaching. Moreover, the switching speed of our 3DOM films increases as pore size decreases. As discussed above, the switching speed of  $V_2O_5$  films depends on three parameters:  $Li^+$  diffusion coefficient,  $Li^+$  diffusion distance, and electrical conductivity<sup>22-24</sup>. 3DOM structures can enhance the crystallinity of  $V_2O_5$  films, then improving the electron conductivity for effective electrochromic reactions<sup>22, 48</sup>. Interconnected macroporous structures can significantly decrease  $Li^+$  diffusion distances by maintaining large active surface areas and low mass transport resistances.

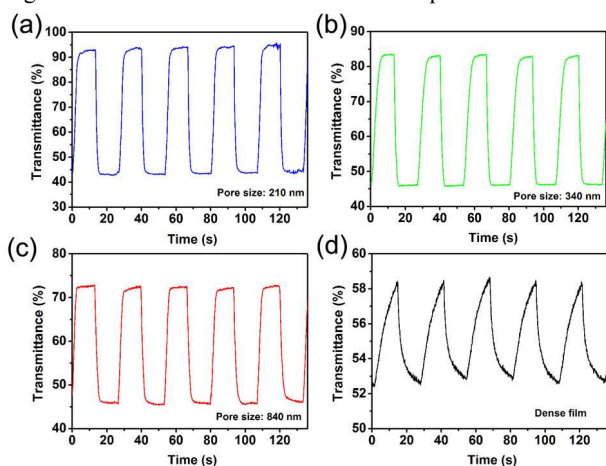


**Fig. 5** Switching response curves of the 3DOM  $V_2O_5$  films with various pore sizes: (a) 210 nm, (b) 340 nm, and (c) 840 nm. The switching response of dense  $V_2O_5$  film is shown in (d).

**Table 2.**

Switching response of 3DOM and dense  $V_2O_5$  films

Sample	Coloration time (s)	Bleaching time(s)
Pore size: 210 nm	1.7	3.2
Pore size: 340 nm	2.2	5.7
Pore size:840 nm	3.0	3.5
Dense film	13.1	13.5

Because of the wide application potential of 3DOM structures in the fields of electrochromism, batteries, and supercapacitors, it is of importance that the effects of 3DOM structures on  $Li^+$  diffusion coefficients be investigated. Chronoamperometry is a

useful technology for investigating  $Li^+$  diffusion coefficients in porous electrodes<sup>52, 53</sup>. Under diffusion-limited conditions, the chronocoulometric response can be described by the following equation:

$$Q = 2n^{-1/2}FAD^{1/2}C_0t^{1/2} + Q_{dl} + nFA\Gamma \quad (8)$$

where  $Q$  is the integrated charge,  $A$  is the electrode area,  $D$  is the chemical diffusion coefficient,  $C_0$  is the ion surface concentration,  $Q_{dl}$  is the double-layer charging, and  $\Gamma$  is the concentration of adsorbed species taking part in the faradic reaction.

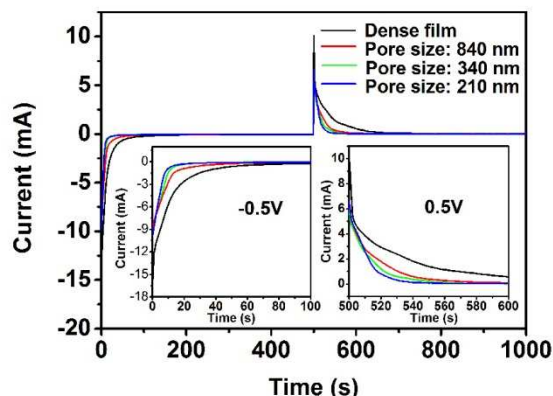


**Fig. 6** Chronoamperometric response curves of the 3DOM  $V_2O_5$  films and that of the dense  $V_2O_5$  film in the potential region of -0.5 V to +0.5 V.

Fig. 6 shows the chronoamperometric response curves of  $V_2O_5$  films in the potential region of 0.5 V to -0.5 V. Consistent with the switching response results, the measured currents of the 3DOM  $V_2O_5$  films decline faster than those of the dense film. 3DOM  $V_2O_5$  films with smaller pores exhibit faster current decreases. The slopes obtained from the  $Q-t^{1/2}$  plots of the intercalation and de-intercalation processes for the  $V_2O_5$  films are plotted in Fig. 7. The slope is identified as  $2n^{-1/2}FAD^{1/2}C_0$ , according to eq. 8. The fit curves of the intercalation and de-intercalation processes of the dense film show axial symmetry about  $y = 0$  while the 3DOM films do not, indicating that the incorporation of 3DOM structures significantly impacts  $Li^+$  diffusion behavior. The slopes of the 3DOM films increase with decreasing pore size, implying that  $Li^+$  intercalation/de-intercalation is easier in 3DOM films with smaller pores. As demonstrated by the CV curves, four couples of redox peaks are present in the potential region of 0.5 V to -0.5 V; therefore,  $n$  equals 3. The diffusion coefficients calculated from Fig. 7 are shown in Table 3. From Table 3, we can see that the diffusion coefficients of intercalation and de-intercalation are enhanced by the 3DOM structure. The  $Li^+$  diffusion coefficient in the ion intercalation process is greater than that of the de-intercalation process, making coloration time shorter than bleaching time. During the  $Li^+$  intercalation process, the 3DOM  $V_2O_5$  film with a pore size of 210 nm has a very high  $Li^+$  diffusion coefficient ( $3.78 \times 10^{-9} \text{ cm}^2/\text{s}$ ), 10.4 times greater than that of the dense  $V_2O_5$  film ( $3.63 \times 10^{-10} \text{ cm}^2/\text{s}$ ). Seman *et al.*<sup>54</sup> reported a diffusion coefficient of  $1 \times 10^{-11} \text{ cm}^2/\text{s}$  for a  $V_2O_5$  film prepared by plasma-enhanced CVD. McGraw *et al.*<sup>44</sup> reported a diffusion coefficient of  $1.7 \times 10^{-12} \text{ cm}^2/\text{s}$  in a  $V_2O_5$  film deposited by PLD. More interesting is that the  $Li^+$  diffusion coefficient of our 3DOM film

with a pore size of 210 nm is much larger than that reported for  $V_2O_5$  nanowires ( $5.3 \times 10^{-10} \text{ cm}^2/\text{s}$ )<sup>18</sup> and comparable to that reported for a  $V_2O_5/\text{CNT}$  composite ( $3 \times 10^{-9} \text{ cm}^2/\text{s}$ )<sup>45</sup>. Due to its significantly enhanced  $\text{Li}^+$  diffusion coefficient, this 3DOM  $V_2O_5$  film has significant potential for lithium-ion applications, such as electrochromics, lithium ion batteries, supercapacitors, and sensors.

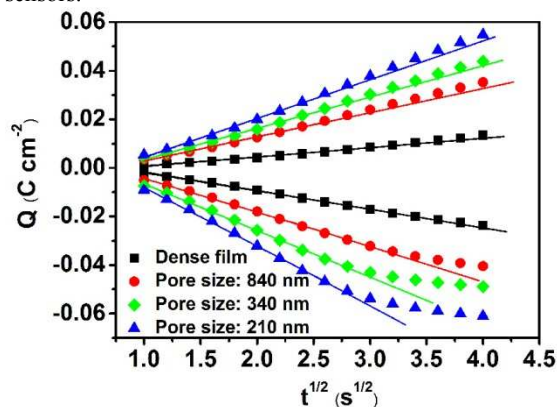


Fig. 7 Plot illustrating differences in ion transport and electron transport rates in the dense film and 3DOM  $V_2O_5$  films.

Table 3

Diffusion coefficient measured from the chronoamperometric response curves

Sample	Diffusion coefficient of $\text{Li}^+$ ( $\text{cm}^2/\text{s}$ )	
	intercalation	de-intercalation
Pore size: 210nm	$3.78 \times 10^{-9}$	$1.68 \times 10^{-9}$
Pore size: 340nm	$2.42 \times 10^{-9}$	$1.07 \times 10^{-9}$
Pore size: 840nm	$1.25 \times 10^{-9}$	$6.51 \times 10^{-10}$
Dense film	$3.63 \times 10^{-10}$	$9.11 \times 10^{-11}$

The influence of the 3DOM structure on  $\text{Li}^+$  intercalation/de-intercalation behaviors manifests in at least three aspects. Fig. 8 illustrates the influence of the 3DOM structure on these behaviors. Firstly, sharp nanoscale edges reduce the polarization of the electrode. Derived from the 3D ordered structure of the colloidal crystal template, 3DOM  $V_2O_5$  exhibits two types of porosity: large macropores, formed by the PS spheres, and smaller mesopores, formed by the contact points between the spheres. The two-type interconnected porous structure has various sharp nanoscale edges around pores which uniformly distribute throughout the film. Upon application of a potential, a relatively high strength electric field situates at these sharp nanoscale edges, resulting in a weaker electric field in the remaining surface and releasing the polarization there. Taking into account the fact that the surface area of the sharp edges is only a small portion of the total surface area, 3DOM films can decrease polarization within the electrode, facilitating  $\text{Li}^+$  intercalation/de-intercalation processes. Secondly, surface roughness improves lithium ion intercalation and de-intercalation. Rough surfaces work to the advantage of  $\text{Li}^+$  intercalation and de-intercalation because they create more defects for lithium ions to quickly intercalate/de-intercalate electrodes<sup>22</sup>, minimizing the effects of sluggish solid-state ion transport. Finally, nanocrystals in the 3D framework facilitate the electron transport during electrochromic reactions<sup>22, 23, 48</sup>. Confined deposition of  $V_2O_5$  into colloidal-crystal-template voids leads to nanocrystals in the wall surface, which improve the

electrical conductivity. Because electrochromic reactions are double injection of ions and electrons, thus the improved electrical conductivity can accelerate the electrochromic reaction rate. From the above discussion, it can be concluded that the mechanism by which both electrons and ions react and are transported in 3DOM structures is 3-dimensional. Contrarily, in nanofiber-structured electrodes, although ions can diffuse into the nanofibers 3-dimensionally, axial electron transport is 1D.

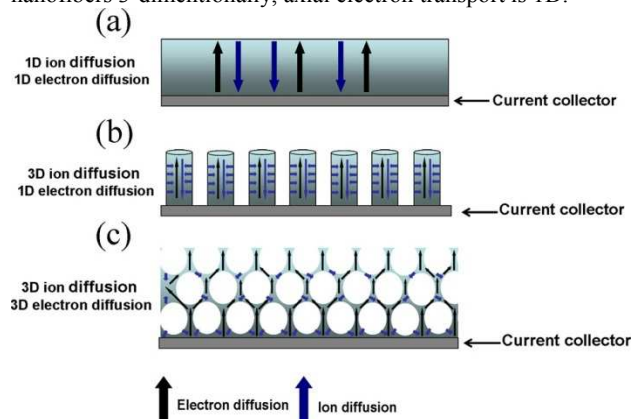


Fig. 8 Schematics illustrating the differences between ion transport and electron transport in dense films, nanofibers and 3DOM films.

## Conclusions

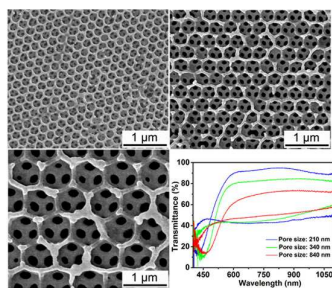
Three-dimensionally ordered macroporous (3DOM)  $V_2O_5$  films with various pore diameters were successfully fabricated through anodic deposition of  $V_2O_5$  into colloidal crystal templates. The influences of 3DOM structures on the electrochromic performance and lithium ion diffusion behaviors were discussed. Small pore size leads to plenty of  $\text{Li}^+$  intercalation sites and thin network walls, resulting in high optical contrast and fast switching response. 3DOM  $V_2O_5$  film with a pore size of 210 nm exhibits highly enhanced transmittance modulation in the visible and NIR spectral regions (50 % at  $\lambda = 650 \text{ nm}$  and 47 % at  $\lambda = 900 \text{ nm}$ ) and fast response times (1.7 s for coloration and 3.2 s for bleaching). Moreover, such film demonstrates a very high  $\text{Li}^+$  diffusion coefficient of  $3.78 \times 10^{-9} \text{ cm}^2/\text{s}$ , which is 10.4 times higher than that of the dense  $V_2O_5$  film ( $3.63 \times 10^{-10} \text{ cm}^2/\text{s}$ ). Three factors are responsible for these improved  $\text{Li}^+$  diffusion behaviors. Sharp nanoscale edges reduce polarization of the electrode; surface roughness improves the ease of lithium ion intercalation and de-intercalation; nanocrystals in the 3D framework facilitate the electron transport during electrochromic reactions.

## Acknowledgements

We thank National Natural Science Foundation of China (No. 51010005, 90916020, 51174063), the Program for New Century Excellent Talents in University (NCET-08-0168), Natural Science Funds for Distinguished Young Scholar of Heilongjiang province, and the project of International Cooperation supported by Ministry of Science and Technology of China (2013DFR10630)

## Notes and references

- †  
‡  
§  
||
- <sup>a</sup> Center for Composite Material, Harbin Institute of Technology, Harbin, China. Fax: 086 45186402345; Tel: 086 451 86402345; E-mail: [yaoli@hit.edu.cn](mailto:yaoli@hit.edu.cn)
- <sup>b</sup> School of Chemical Engineering and Technology, Harbin Institute of Technology, 150001, Harbin, China. E-mail: [jpzhaoh@hit.edu.cn](mailto:jpzhaoh@hit.edu.cn)
- <sup>c</sup> Laboratory of Inorganic Materials Chemistry (CMI), University of Namur, 61, rue de Bruxelles, B-5000 Namur, Belgium.
- 1 D. R. Rosseinsky and R. J. Mortimer, *Adv. Mater.*, 2001, **13**, 783.  
 2 C. G. Granqvist, *Nat. Mater.*, 2006, **5**, 89.  
 3 C. G. Granqvist, *Sol. Energy Mater. Sol. Cells*, 2012, **99**, 1.  
 4 H. Demiryont and D. Moorehead, *Sol. Energy Mater. Sol. Cells*, 2009, **93**, 2075.  
 5 N. M. Vuong, D. Kim and H. Kim, *J. Mater. Chem. C*, 2013, **1**, 3399.  
 6 K. Y. Lee, D. Kim, S. Berger, R. Kirchgeorg and P. Schmuki, *J. Mater. Chem.*, 2012, **22**, 9821.  
 7 Y. Yang, D. Kim, P. Schmuki, *Electrochem. Commun.*, 2011, **13**, 1198.  
 8 D. S. Dalavi, R. S. Devan, R. S. Patil, Y.-R. Ma, M.-G. Kang, J.-H. Kim and P. S. Patil, *J. Mater. Chem. A*, 2013, **1**, 1035  
 9 S. I. Cho, W. J. Kwon, S. J. Choi, P. Kim, S. A. Park, J. Kim, S. J. Son, R. Xiao, S. H. Kim and S. B. Lee, *Adv. Mater.*, 2005, **17**, 171.  
 10 Y. Wang and G. Cao, *Chem. Mater.*, 2006, **18**, 2787.  
 11 Y. Wang, K. Takahashi, K. Lee and G. Cao, *Adv. Funct. Mater.*, 2006, **16**, 1133.  
 12 Y. Yang, D. Kim and P. Schmuki, *Electrochem. Commun.*, 2011, **13**, 1021.  
 13 Y.-S. Lin and C.-W. Tsai, *Surf. Coat. Technol.*, 2008, **202**, 5641.  
 14 H. G. Wei, X. R. Yan, S. J. Wu, Z. P. Luo, S. Y. Wei and Z. H. Guo, *J. Phys. Chem. C*, 2012, **116**, 25052.  
 15 G. F. Cai, J. P. Tu, C. D. Gu, J. H. Zhang, J. Chen, D. Zhou, S. J. Shi and X. L. Wang, *J. Mater. Chem. A*, 2013, **1**, 4286.  
 16 G. F. Cai, J. P. Tu, D. Zhou, J. H. Zhang, Q. Q. Xiong, X. Y. Zhao, X. L. Wang and C. D. Gu, *J. Phys. Chem. C*, 2013, **117**, 15967.  
 17 R. A. Patil, R. S. Devan, J. H. Lin, Y. R. Ma, P. S. Patil and Y. Liou, *Sol. Energy Mater. Sol. Cells*, 2013, **112**, 91.  
 18 C. R. Xiong, A. E. Aliev, B. Gnade and K. J. Balkus, Jr., *ACS Nano*, 2008, **2**, 293.  
 19 J.-W. Liu, J. Zheng, J.-L. Wang, J. Xu, H.-H. Li and S.-H. Yu, *Nano Lett.*, 2013, **13**, 3589.  
 20 X. W. Sun and J. X. Wang, *Nano Lett.*, 2008, **8**, 1884.  
 21 D.-H. Kim, *Sol. Energy Mater. Sol. Cells*, 2012, **107**, 81.  
 22 E. M. Sorensen, S. J. Barry, H.-K. Jung, J. R. Rondinelli, J. T. Vaughry and K. R. Poeppelmeier, *Chem. Mater.*, 2006, **18**, 482.  
 23 M. R. J. Scherer, L. Li, P. M. S. Cunha, O. A. Scherman and U. Steiner, *Adv. Mater.*, 2012, **24**, 1217.  
 24 D. Wei, M. R. J. Scherer, C. Bower, P. Andrew, T. Ryhanen and U. Steiner, *Nano Lett.*, 2012, **12**, 1857.  
 25 M. R. J. Scherer and U. steiner, *Nano Lett.*, 2013, **13**, 3005.  
 26 Y. Xia, B. Gates, Y. Yin and Yu Lu, *Adv. Mater.*, 2000, **12**, 693.  
 27 A. Stein, F. Li and N. R. Denny, *Chem. Mater.*, 2008, **20**, 649.  
 28 A. Stein, B. E. Wilson and S. G. Rudisill, *Chem. Soc. Rev.*, 2013, **42**, 2763.  
 29 A. Blanco, E. Chomski, S. Grabtchak, M. Ibisate, S. John, S. W. Leonard, C. Lopez, F. Meseguer, H. Miguez, J. P. Mondia, G. A. Ozin, O. Toader and H. M. van Driel, *Nature*, 2000, **405**, 437.  
 30 S. K. Karuturi, L. Liu, L. T. Su, A. Chutinan, N. P. Kherani, T. K. Chan, T. Osipowicz and A. I. Y. Tok, *Nanoscale*, 2011, **3**, 4951.  
 31 H. W. Zhang, G. T. Duan, G. Q. Liu, Y. Li, X. X. Xu, Z. F. Dai, J.J. Wang and W. P. Cai, *Nanoscale*, 2013, **5**, 2460.  
 32 L. L. Yang, D. T. Ge, J. P. Zhao, Y. B. Ding, X. P. Kong and Y. Li, *Sol. Energy Mater. Sol. Cells*, 2012, **100**, 251.  
 33 L. Li, U. Steiner and S. Mahajan, *J. Mater. Chem.*, 2010, **20**, 7131.  
 34 J. Zhang, J. P. Tu, G. F. Cai, G. H. Du, X. L. Wang and P. C. Liu, *Electrochim. Acta*, 2013, **99**, 1.  
 35 J. H. Kim, S. H. Kang, K. Zhu, J. Y. Kim, N. R. Neale and A. J. Frank, *Chem. Commun.*, 2011, **47**, 5214.  
 36 X.-H. Xia, J.-P. Tu, X.-L. Wang, C.-D. Gu and X.-B. Zhao, *J. Mater. Chem.*, 2011, **21**, 671.  
 37 C.-H. Huang, Q. Zhang, T.-C. Chou, C.-M. Chen, D. S. Su and R.-A. Doong, *ChemSusChem*, 2012, **5**, 563.  
 38 L. Liu, S. K. Karuturi, L. T. Su and A. I. Y. Tok, *Energy Environ. Sci.*, 2011, **4**, 209.  
 39 J. P. Bosco, K. Sasaki, M. Sadakane, W. Ueda and J. G. Chen, *Chem. Mater.*, 2010, **22**, 966.  
 40 K. Takahashi, Y. Wang and G. Cao, *Appl. Phys. Lett.*, 2005, **86**, 053102.  
 41 Y. Y. Liu, M. Clark, Q. F. Zhang, D. M. Yu, D. W. Liu, J. Liu and G. Cao, *Adv. Energy Mater.*, 2011, **1**, 194.  
 42 V. Modafferi, G. Panzera, A. Donato, P. L. Antonucci, C. Cannilla, N. Donato, D. Spadaro and G. Neri, *Sens. Actuators, B*, 2012, **163**, 61.  
 43 E. Portiron, A. L. Salle, A. Varbaere, Y. Piffard, and D. Guyomard, *Electrochim. Acta*, 1999, **45**, 197.  
 44 J. M. McGraw, C. S. Bahn, P. A. Parilla, J. D. Perkins, D. W. Readey and D.S. Ginley, *Electrochim. Acta*, 1999, **45**, 187.  
 45 D. A. Semenenko, T. L. Kulova, A. M. Skundin, D. M. Itkis, E. A. Pomerantseva, E. A. Goodilin and Y. D. Tretyakov, *Mendeleev Commun.*, 2010, **20**, 12.  
 46 M. A. McLachlan, N. P. Johnson, R. M. Rue La De and D. W. McComb, *J. Mater. Chem.*, 2004, **14**, 144.  
 47 G. Bar, N. Larina, L. Grinis, V. Kokshin, R. Gvishi, I. Kiryushev, A. Zaban and V. Khodorkovsky, *Sol. Energy Mater. Sol. Cells*, 2012, **99**, 123.  
 48 L. Michailovits, K. Bali, T. Szörényi, and I. Hevesi, *Acta Physica Academiae Scientiarum Hungaricae*, 1980, **49**, 217.  
 49 Y. Y. Liu, M. Clark, Q. F. Zhang, D. M. Yu, D. W. Liu, J. Liu and G. Cao, *Adv. Energy Mater.*, 2011, **1**, 194.  
 50 C. K. Chan, H. L. Peng, R. D. Twesten, K. Jarausch, X. F. Zhang and Y. Cui, *Nano Lett.*, 2007, **7**, 490.  
 51 K. C. Cheng, F. R. Chen and J. J. Kai, *Sol. Energy Mater. Sol. Cells*, 2006, **90**, 1156.  
 52 H. Lindstrom, S. Sodergren, A. Solbrand, H. Rensmo, J. Hjelm, A. Hagfeldt and S.-E. Lindquist, *J. Phys. Chem. B*, 1997, **101**, 7710.  
 53 J. Liu and A. Manthiram, *J. Electrochem. Soc.*, 2009, **156**, A833.  
 54 M. Seman, J. Marino, W. Yang and C. A. Wolden, *J. Non-Cryst. Solids*, 2005, **351**, 1987.



Electrodeposited 3D ordered macroporous V<sub>2</sub>O<sub>5</sub> film contains nanocrystallites and amorphous parts, and exhibits improved electrochromic performance and lithium diffusion coefficient.